

This work was written as part of one of the author's official duties as an Employee of the United States Government and is therefore a work of the United States Government. In accordance with 17 U.S.C. 105, no copyright protection is available for such works under U.S. Law.

Public Domain Mark 1.0

<https://creativecommons.org/publicdomain/mark/1.0/>

Access to this work was provided by the University of Maryland, Baltimore County (UMBC) ScholarWorks@UMBC digital repository on the Maryland Shared Open Access (MD-SOAR) platform.

Please provide feedback

Please support the ScholarWorks@UMBC repository by emailing scholarworks-group@umbc.edu and telling us what having access to this work means to you and why it's important to you. Thank you.

Multiscale, multipoint measurements from Cluster: Advancing our scientific understanding of geospace

M.L. Goldstein ^{a,*}, C.P. Escoubet ^b, H. Laakso ^b

^a Code 692, NASA Goddard Space Flight Center, Greenbelt, MD 20771, USA

^b ESA/ESTEC, SCI-SH, Keplerlaan 1, 2200 AG Noordwijk, The Netherlands

Received 6 December 2004; received in revised form 11 January 2005; accepted 11 January 2005

Abstract

Cluster is the first multispacecraft mission with identical instrumentation designed to resolve spatial and temporal structures in geospace. The orbits of the four Cluster spacecraft are variable and are adjusted periodically to place the spacecraft into configurations that optimize the three-dimensional capabilities of the instrumentation. During the mission, the relative distances between the spacecraft achieved so far have ranged from 100 to 5000 km. In the summer of 2005, the maximum separations were increased to 10,000 km. The primary results of Cluster include: determining the spatial scales of such transient three-dimensional phenomena as the short large amplitude magnetic structures (SLAMS) ahead of the parallel bow shock, the scale of Earth's bow shock, the properties of bursty bulk flows in the plasmashet, detailed measurements of the diffusion regions characteristic of magnetic reconnection events both in the magnetotail, at the magnetopause, and in the dayside polar cusps, and determinations of the source locations of both continuum radiation and auroral kilometric radiation. Space restrictions only permit a subset of those results to be mentioned.

© 2006 COSPAR. Published by Elsevier Ltd. All rights reserved.

Keywords: Cluster mission; Magnetosphere boundaries; Multi-point measurements; Magnetosphere dynamics; Magnetosphere structure

1. Introduction

Not long after the general structure of Earth's magnetosphere was determined, Jim Dungey (Fig. 1), who was among the first to describe the importance of the interplanetary magnetic field and magnetic reconnection in transferring energy from the solar wind into the polar auroral zones, anticipated the need for multiple space probes in his inaugural lecture at Imperial College in May 1966:

Looking to the future, I believe that progress requires bunches of satellites, though these are as yet in no published program... For any magnetic disturbance it would be extremely useful to obtain the curl of the magnetic field because this tells one the current.

Cluster, while not the first multispacecraft mission, is the first mission to deploy four identically instrumented spacecraft with orbits arranged so that the spacecraft can occupy the vertices of a tetrahedron in space. This arrangement permits time and space to be disentangled and allows for the determination of the thickness and motion of boundaries. Often, the orbital configuration enables one to determine the three-dimensional structure of many regions of geospace. When the spacecraft configuration approximates the vertices of a regular tetrahedron, measurements of the magnetic field at the four locations can be used to construct the curl of the magnetic field, and thus, the current (see Fig. 2).

The Cluster mission was first proposed more than 20 years ago in response to an ESA call for proposals. Earlier, NASA had studied a related concept of a Turbulence Explorer mission. The mission concept was further refined under the umbrella of NASA's Cooperative Solar Terrestrial Research (COSTR). At the end of 1985 the Cluster mission was presented to the scientific community and in

* Corresponding author.

E-mail address: melvyn.goldstein@gsfc.nasa.gov (M.L. Goldstein).



Fig. 1. Jim Dungey near Ashkelon during a visit to Israel, circa 1971 (picture taken by one of the authors (MLG)).

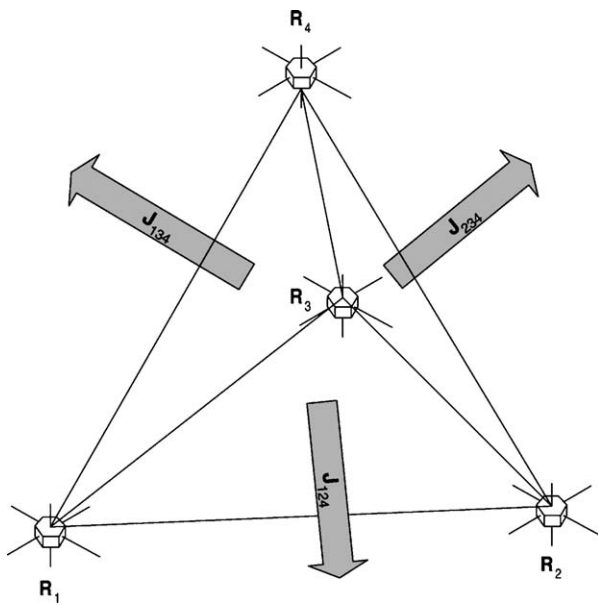


Fig. 2. A schematic of the curlometer technique using the magnetic field data from four spacecraft located at the vertices of a regular tetrahedron (Robert et al., 1998; Dunlop et al., 2002).

February 1986, the Solar Terrestrial Science Program (STSP) program, combining both Cluster and SOHO missions, was selected by the ESA Science Program Committee. After a joint ESA/NASA Announcement of Opportunity issued in March 1987, the 11 instruments making up the scientific payload were selected in March 1988. Unfortunately, the launch with the first Ariane 5 on 4 June 1996 failed when the rocket exploded 47 s after lift-off. After considerable work, the ESA Science Program Committee (SPC) agreed in April 1997 to reflly the mission

and Cluster II was born (Escoubet et al., 2001). The first launch of a Soyuz containing the initial pair of spacecraft was on July 16, 2000 from the Baikonur Cosmodrome. The second pair was launched August 9, 2000, also from Baikonur on a Soyuz. The official science investigations began on February 1, 2001. In February 2002 ESA approved a 35-month continuation of Cluster. A further mission extension for an additional four years has been approved by ESA (Fig. 3).

2. Overview of the Cluster mission

The scientific objectives of Cluster mission are to study the small-scale structures and the turbulence in the key regions of the magnetosphere. These regions include the solar wind, the bow shock, the magnetopause, the polar cusp, and the magnetotail. In addition, the temporal variations of structures observed in the auroral zone, mid-altitude polar cusp, and plasmasphere can be studied when the spacecraft trajectories form a “string of pearls” near perigee.

The Cluster spacecraft are in $4 \times 19.6R_E$ polar orbits that are adjusted periodically to form perfect tetrahedra in key regions such as the polar cusps and plasmasheet.

The perfect tetrahedron occurs only twice per orbit for a limited period of time ($\sim 5\text{--}6$ h along the 56-h orbit). For the remainder of the orbit, the tetrahedron is distorted, more akin to a *string-of-pearls* configuration near perigee.

The separation distance (estimated when the tetrahedron is most regular) has been changed several times since the mission began (Table 1). In the northern hemisphere spring, apogee is in the solar wind and the Cluster orbits are optimized for studies of the cusp, bow shock, solar wind, and other dayside phenomena. In the northern hemisphere fall the orbits are similarly optimized for studies of the plasmasheet and other regions in the magnetotail (Fig. 4).

Once the separation is moved to 10,000 km (or more), nearly all the on-board fuel will have been consumed and further adjustments of the separation distance will, of necessity, be small. After early 2003, the constellation maneuvers have been carried out only once a year to decrease the operational costs and to minimize data-collection interruptions. The Flight Dynamics Team at the European Space Operations Centre (ESOC) has developed a way to simultaneously configure a tetrahedron both in the tail and in the northern polar region, thereby covering both the tail and the northern cusp without additional orbit modifications. The small separation distances in the magnetotail (August 2003) made it possible to investigate two competing processes that might produce geomagnetic substorms, viz., magnetic reconnection and current disruption. The existence of a small “diffusion” region where the plasma is rapidly accelerated is expected in the first model, while a disruption of cross-tail current is expected in the second model. Both phenomena have a scale size of ~ 500 km.

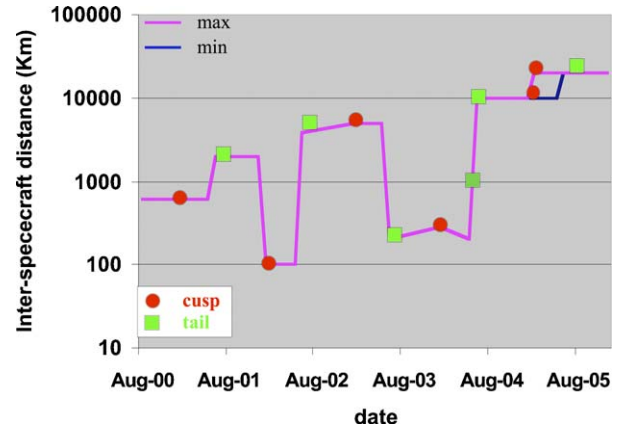
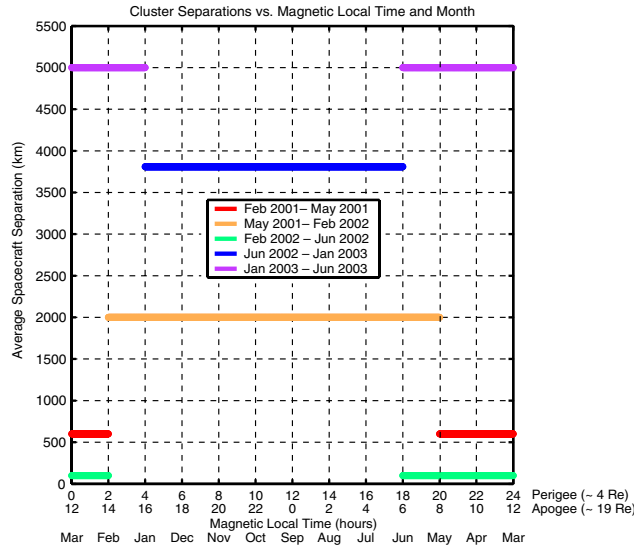


Fig. 3. Two graphical representation of the Cluster separations. On the left, the separations are plotted against magnetic local time (MLT), while on the right, the separations show the regions designated for study (red for the cusp, green for the tail). (For interpretation of the references to color in this figure legend, the reader is referred to the web version of this paper.)

Table 1
Spacecraft separations

Year	Phase	Separation (km)
2001	Cusp	600
2001	Tail	2,000
2002	Cusp	100
2002	Tail	4,000
2003	Cusp	5,000
2003	Tail	200
2004	Cusp	300
2004	Tail	1000
2005	Cusp	13,000
2005	Tail	10,000

The data return from Cluster has been augmented by the addition of a second ground-station in Maspalomas (Spain). Since June 2002 the data coverage of Cluster has been 100% (before that, the coverage was $\sim 50\%$). Examples of the data return before and after the data coverage

became 100% are shown in Fig. 5. These Master Science Plan plots provide a summary of mission observations. The plots show a series of orbits with orbit number increasing from left to right. Individual orbits are plotted from perigee (bottom) outbound to apogee (middle) and then inbound to the next perigee (top).

3. A sampling of science results

3.1. Quasi-perpendicular bow shock crossings

Fig. 6 shows three samples of a two-dimensional cut in the $v_{\text{sw}} - B$ plane through phase space distributions of H^+ at a quasi-perpendicular bow shock with Alfvénic Mach number $M_A = 5.6$ observed on January 2, 2002 from 14:42–14:48 UT. A reflected beam is seen upstream whose emergence out of the gyrating ions can be seen in the ramp. Both distributions are taken simultaneously on C1 and C3. A highly anisotropic distribution is observed downstream

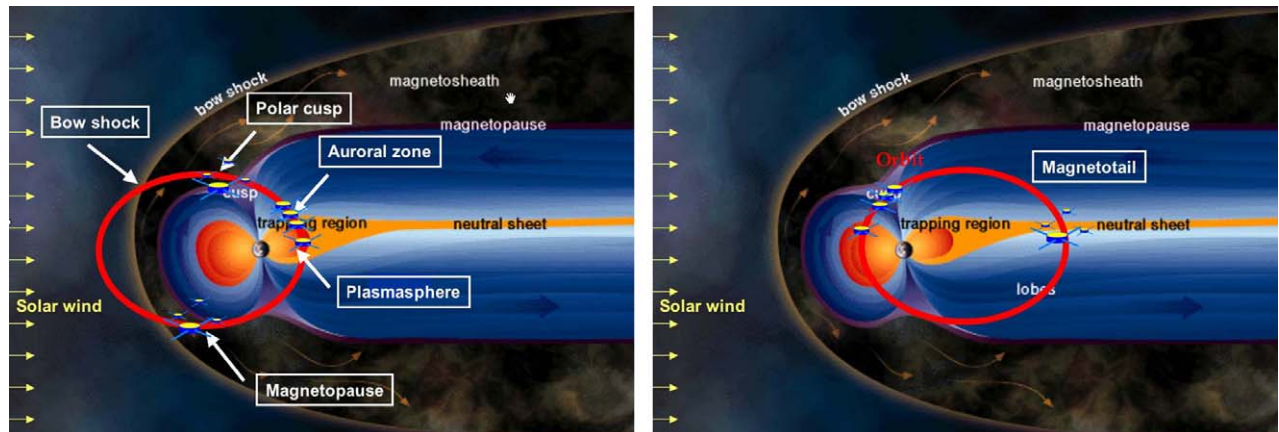


Fig. 4. Regions visited in the northern hemisphere spring (left) and northern hemisphere fall (right).

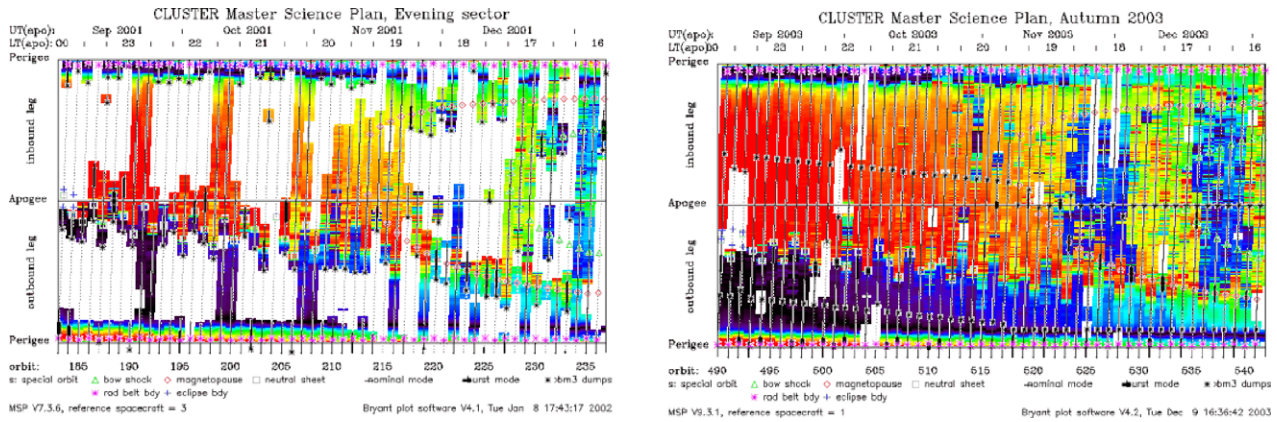


Fig. 5. Left: Master science plan showing the $\sim 50\%$ data coverage during commissioning. Right: Master Science plan showing regions visited with nearly 100% data coverage (archives of the Master Science plans can be found at http://www.cluster.rl.ac.uk/csdsweb/csdsweb_msparch.htm).

with no particles in the phase space of the beam. These features are seen independently, whether observed consecutively on the same spacecraft or simultaneously on different spacecraft. A second example from a crossing of a quasi-perpendicular bow shock on March 31, 2001 is shown in Fig. 8 from Kucharek et al. (2004). The top panel shows the magnetic field magnitude from FGM. The angle between the shock normal and the magnetic field was estimated to be $\sim 78^\circ$. These observations upstream and downstream of the quasi-perpendicular bow shock indicate that field-aligned beams most likely result from pitch-angle scattering during ion reflection in the shock ramp.

Measurements of the cross shock electric field at a series of low Alfvénic Mach number nearly perpendicular shocks have been reported using EFW. Typical cross-shock potentials in the Normal Incidence Frame (NIF), where the solar wind is directed along the shock normal, range from 0.5 to 0.8 times the ion energy change. Fig. 7 shows the integrated electric potential (top panel) in the NIF, the electric field both the NIF and spacecraft frames of reference, and the spacecraft potential. The cross-shock potential slows the incoming solar wind protons, accelerates electrons, and helps to reflect the ions, thus controlling the reflection efficiency (Fig. 9).

Measurements of the spacecraft potential on the four Cluster spacecraft have also allowed determination of the length scale of the density transition at 98 quasi-perpendicular bow shock crossings. Bale et al. (2003) found that at low (sonic) Mach numbers, M , the density transition is consistent with both ion inertial scales c/ω_{pi} and with convected gyroradii $v_{sh,n}/\Omega_{ci,2}$ (where $v_{sh,n}$ is the shock speed in the plasma frame and $\Omega_{ci,2}$ is the downstream ion gyrofrequency). For $M \geq 4$ –5 the convected gyroradius is the preferred scale for the shock density transition and the inferred scale is $L \approx 0.4v_{sh,n}/\Omega_{ci,2}$ (Fig. 10).

3.2. Short amplitude magnetic structures observed at quasi-parallel bow shock crossings

When θ_{Bn} is less than $\sim 45^\circ$ (referred to as a “quasi-parallel” shock), particles are able to reflect off the shock

structure and propagate upstream. The streaming particles can both generate and interact with waves. For quasi-parallel shocks, the transition from the solar wind to the magnetosheath is extended and chaotic. One way to view this dynamical situation is to think of the shock as undergoing cyclic reformation. The chaotic pattern of magnetic field enhancements are referred to as SLAMS (Short Large-Amplitude Magnetic Structures) (Schwartz, 1991; Schwartz and Burgess, 1991; Scholer and Burgess, 1992; Giacalone et al., 1993). The magnetic field magnitude of SLAMS is required to be at least a factor of 2.5 larger than the undisturbed field. They sweep past the spacecraft within ~ 10 s. Although SLAMS propagate sunward in the plasma frame, they are convected anti-sunward by the solar wind. In Fig. 11 (Lucek et al., 2004) two such observations of SLAMS are shown which demonstrate that on the 100 km scale, the magnetic signatures are typically well correlated between the spacecraft, however, significant differences are present between the four spacecraft when the separation is 600 km.

3.3. Cluster as a wave telescope

Cluster makes it possible with four point measurements of the magnetic field to determine the general polarisation properties of electromagnetic fluctuations. Glassmeier et al. (1995) describe such a technique. The method requires that one knows the wave propagation direction (Pinçon and Lefeuvre, 1991; Motschmann et al., 1996; Motschmann et al., 1998) and allows one to calculate the energy per eigenmode of a given wave field for a given position in $\omega - k$ space.

Fig. 12 illustrates an example of how the technique can be used to identify wave modes. The left three panels show a fluctuation observed in the spacecraft frame of reference at 0.37 Hz at three k_z planes containing three maxima of magnetic energy. The dispersion curves for the fast, slow, and Alfvén modes are shown in red, the mirror mode is in blue. The isocontours are the experimental results. The max and min values are the maximum and the minimum energy density [$\text{nT}^2/\text{Hz} (\text{rd}/\text{km})^3$] for the given k_z plane.

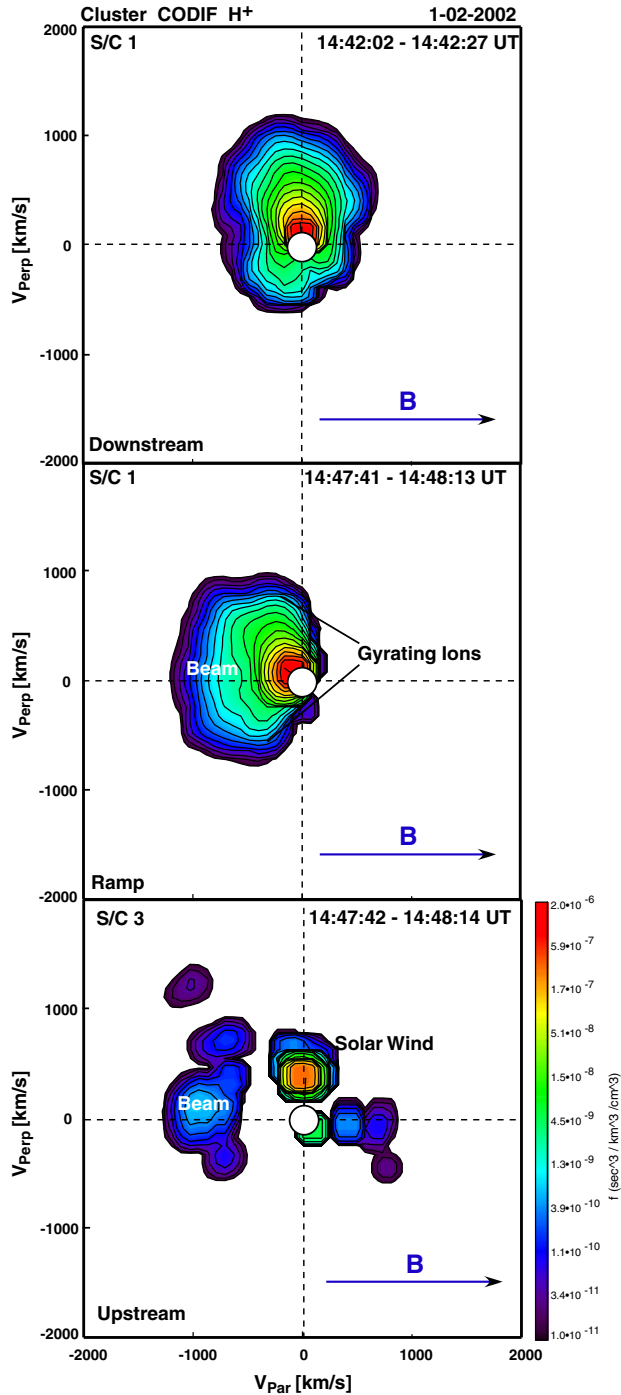


Fig. 6. Two-dimensional cuts of the H^+ phase space distributions at the quasi-perpendicular bow shock crossing on January 2, 2002. Top: downstream of the shock on C1. Center: in the shock ramp on C1. Bottom: upstream of the shock on C3 (adapted from Kucharek et al., 2004).

For the same frequency, magnetic energy is distributed over four wave vectors that are close to the mirror, fast, Alfvén, and slow modes. The right side of Fig. 12 shows a three-dimensional display in k -space for $f_1 = 0.37$ Hz. Energy isocontours for 20 values of k_z are shown. The dense filled regions represent the three significant maxima.

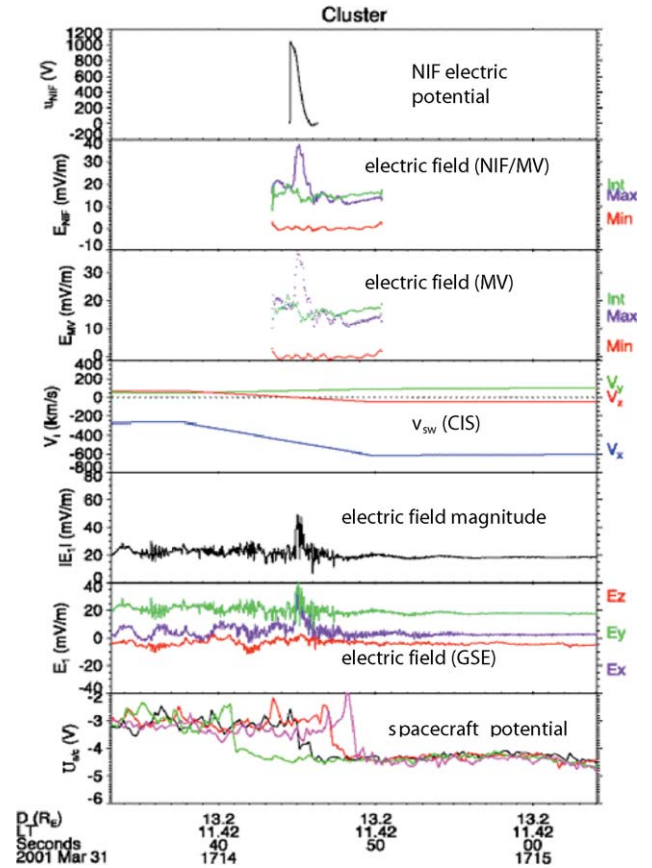


Fig. 7. Electric fields in the GSE and Normal Incidence Frame (NIF) coordinate systems and spacecraft potential and plasma flow at a bow shock crossing also on March 31, 2001. (Figure provided by S. Bale and F. Mozer.)

3.4. Multi-spacecraft, multi-instrument observations of the polar cusp

Cluster has found >40 keV electrons throughout the cusp region on open magnetic field lines. The observations have implications for the topology of the magnetosphere and for the mechanisms responsible either for untrapping the electrons or for accelerating them. Fig. 13 illustrates the conjunction of energetic electrons and ions with the presence of solar wind plasma and depressed magnetic fields in the high-altitude cusp region. [The data shown in Fig. 13 were assembled by D. Winningham for the Cluster submission to the 2003 NASA Senior Review of operating missions.] The event illustrates the capabilities of Cluster, the advantages of using as many of the instruments as possible, and the necessity of visiting such regions with different tetrahedral sizes.

Although the spacecraft passed through regions at slightly different times, they observed nearly the same temporal variations in the energetic electrons, which places significant constraints on their source. The outer boundary between open field lines and purely IMF field lines is not easily discerned because Cluster exits through the center of the cusp indentation. Working backwards from the

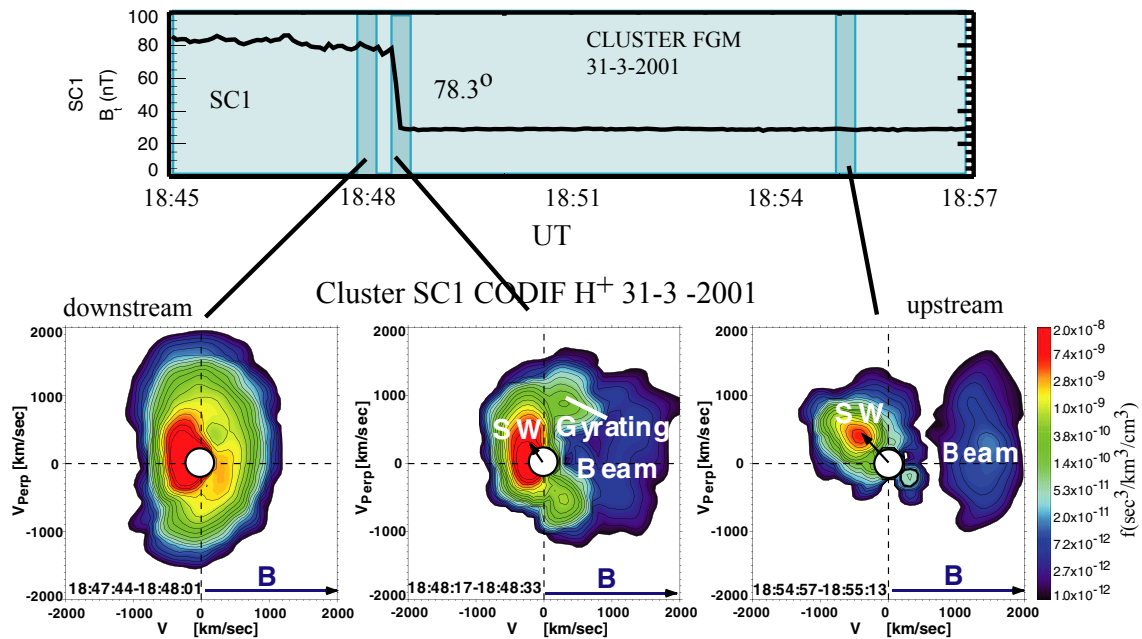


Fig. 8. A crossing of a quasi-perpendicular bow shock on March 31, 2001. The reflected protons are seen several minutes upstream of the shock. In the shock front, the protons have formed a gyrating distribution. The proton observations are from CODIF on Cluster 1. The magnitude of the magnetic field as measured by FGM is shown above the CIS observations (Kucharek et al., 2004).

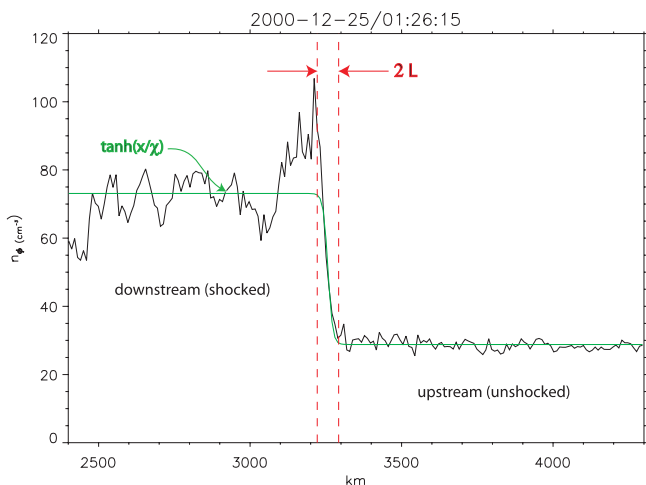


Fig. 9. Density transition from downstream (shocked) to upstream (unshocked) states for a Mach $M \approx 3.5$, $\Theta_{Bn} \approx 81^\circ$ shock. The green line is the hyperbolic tangent fit; red vertical lines show the density transition scale (Bale et al., 2003). (For interpretation of the references to color in this figure legend, the reader is referred to the web version of this paper.)

magnetosheath, the first major departure from magnetosheath (IMF oriented) fields is near 0912 UT, which may be the outer boundary of the cusp. As the spacecraft move inward, the IMF is dominated by B_y . Reconnection in the northern hemisphere should be duskward of noon, well away from the satellite location. The fields and particle fluxes are variable and may be characteristic of a turbulent boundary layer at the outer portion of the cusp cavity. Continuing away from the Sun, Cluster sees the change to negative B_y and positive B_z , which brings the merging

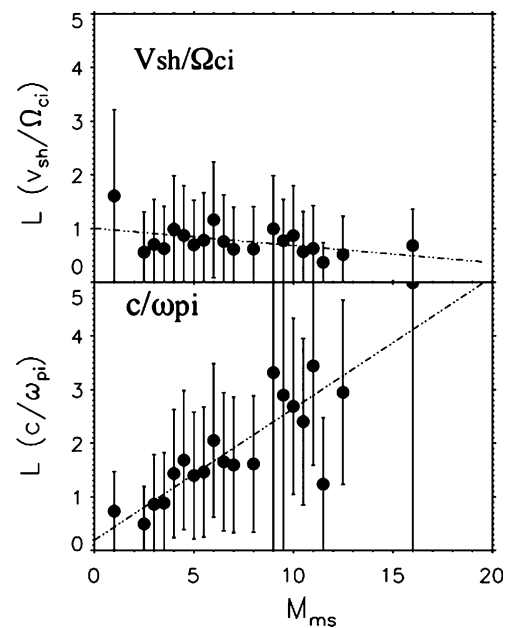


Fig. 10. Relationship between scale size and the magnetosonic Mach number. $L/v_{sh}/\Omega_{ci,2}$ (upper panel) is approximately constant over a large range of Mach number, while the ion inertial scaling (lower panel) increases with Mach number (Bale et al., 2003).

site to the backside of the cusp, pre-noon and in the vicinity of Cluster.

The region labeled mantle appears to be the first excursion into the current layer at the backside of the cusp where reconnection may be occurring above the spacecraft. Both ions and electrons appear to be accelerated, perhaps from

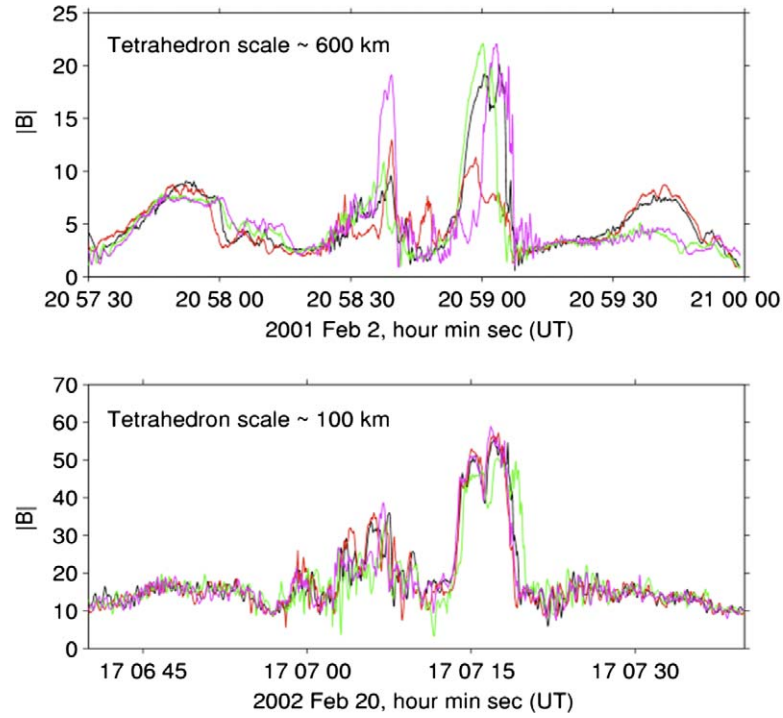


Fig. 11. SLAMS are smaller than had been expected. Here are two examples when the spacecraft were at 600 and 100 km separation. Together the two crossings indicate the true thickness of these structures lies between these two scales (Lucek et al., 2004).

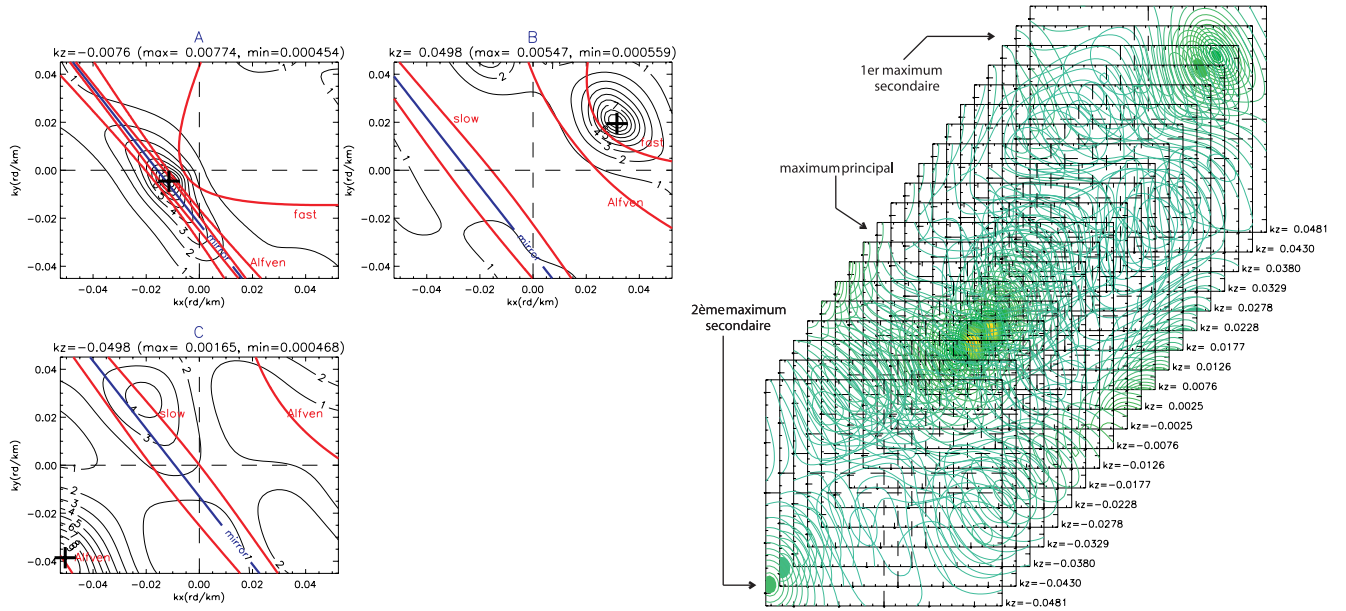


Fig. 12. Left: k -filtering. Right: three-dimensional display of in (k_x, k_y, k_z) space for $f_1 = 0.37$ Hz. Energy isocontours are drawn in (k_x, k_y) planes for 20 values of k_z , k_x and k_y values belong, respectively, to $[-0.0523, 0.0523]$ rd/km and to $[-0.0451, 0.0451]$ rd/km. Filled regions represent the three significant maxima. The color scale goes from red to blue with decreasing energy (Sahraoui et al., 2003). (For interpretation of the references to color in this figure legend, the reader is referred to the web version of this paper.)

reconnection. When the current layer is crossed at 07:55 both ions and electrons show signs of acceleration, indicating that merging has occurred. The region labeled mantle

appears to involve active merging. The broad extent and highly structured nature of this event makes it difficult to define the cusp boundaries.

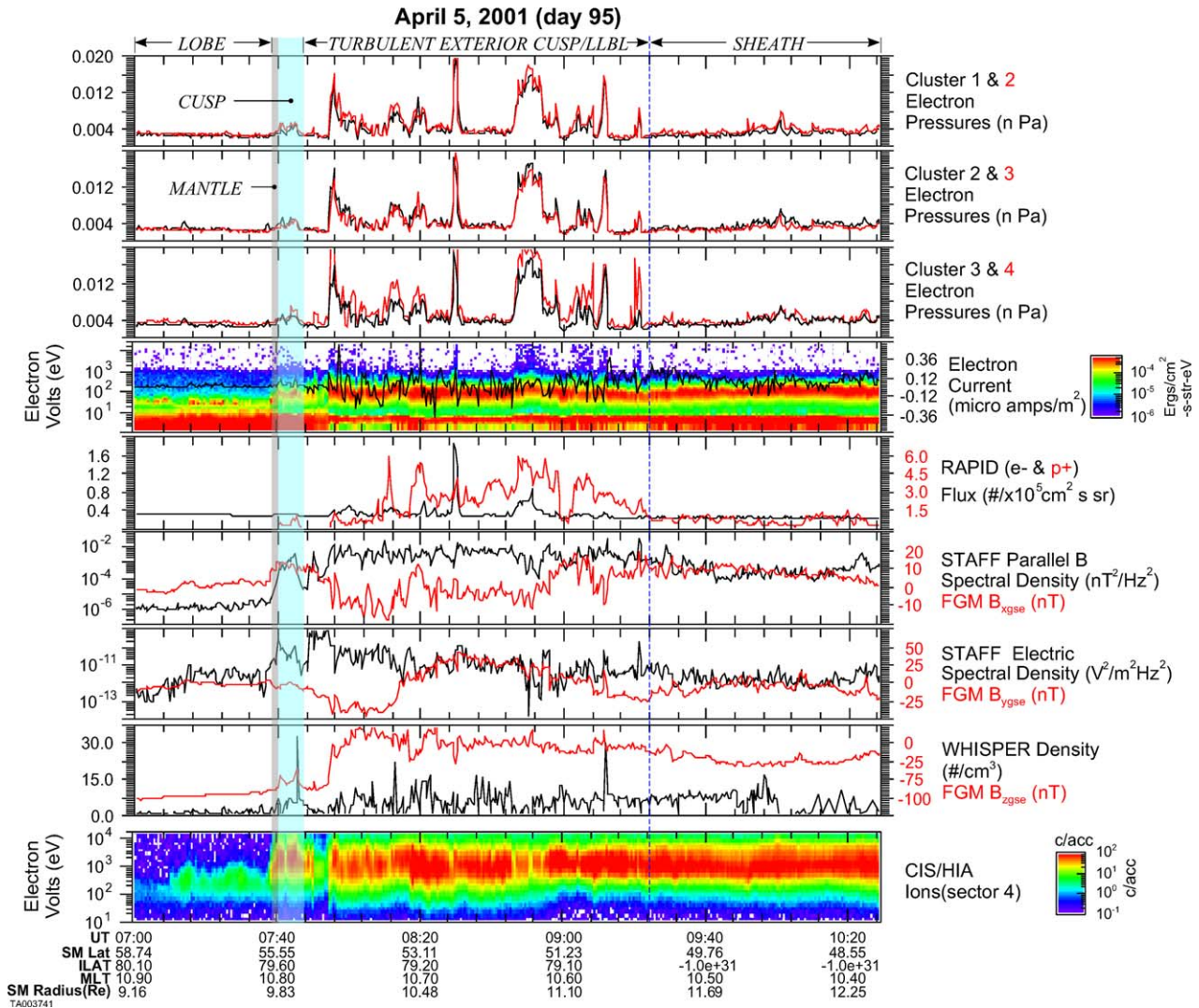


Fig. 13. Electron pressure (nPa) for C1 and C2. Electron pressure C2 and C3. Electron pressure C3 and C4. PEACE electron spectrogram at 0° pitch angle with an overlay of the electron current (μ amps/ m^2). RAPID integral electron fluxes at >30 keV. STAFF B parallel 0.3–10 Hz ULF wave power (black) and FGM B_{xgse} (red). STAFF low frequency electric flux (black) and the FGM B_{ygse} (red). WHISPER plasma density (black) and FGM B_{zgs} (red). CIS/HIA sector 4 ion flux (D. Winningham, private communication). (For interpretation of the references to color in this figure legend, the reader is referred to the web version of this paper.)

3.5. Magnetopause: thickness and currents

A primary objective of Cluster is to measure the currents, thickness, and shape of the magnetopause. Haaland et al. (2004a,b) have analyzed events on March 2, 2002 and July 5, 2001 when the average separation of the spacecraft was 100 km. Using the four spacecraft, the thickness of the magnetopause was found to be a few ion gyroradii (i.e., a few times ≈ 30 km). The density was estimated using data from EFW (Fig. 14). Because the four spacecraft encompassed the current layer, the curlometer technique (Robert et al., 1998; Dunlop et al., 2002) could be used to estimate the current density from $\nabla \times \mathbf{B}$. Various methods were used to compare predictions for determination of the velocity, orientation, speed and thickness of the magnetopause current layer.

3.6. Magnetopause boundary: two-dimensional reconstruction

A recently developed technique for reconstructing approximately two-dimensional (i.e., $\partial/\partial z \approx 0$), time-stationary magnetic field structures in space has been applied by Hasegawa et al. (2004) to two magnetopause traversals on the dawnside flank by Cluster. At that time the spacecraft separation was about 2000 km. The method consists of solving the Grad-Shafranov equation for magnetohydrostatic structures using plasma and magnetic field data measured along a single spacecraft trajectory as spatial initial values.

Two magnetopause crossings (June 30, 2001 and July 5, 2001) were examined and two reconstruction maps were produced, using data from C1 to C3. The correlation coefficient between the predicted and measure field components

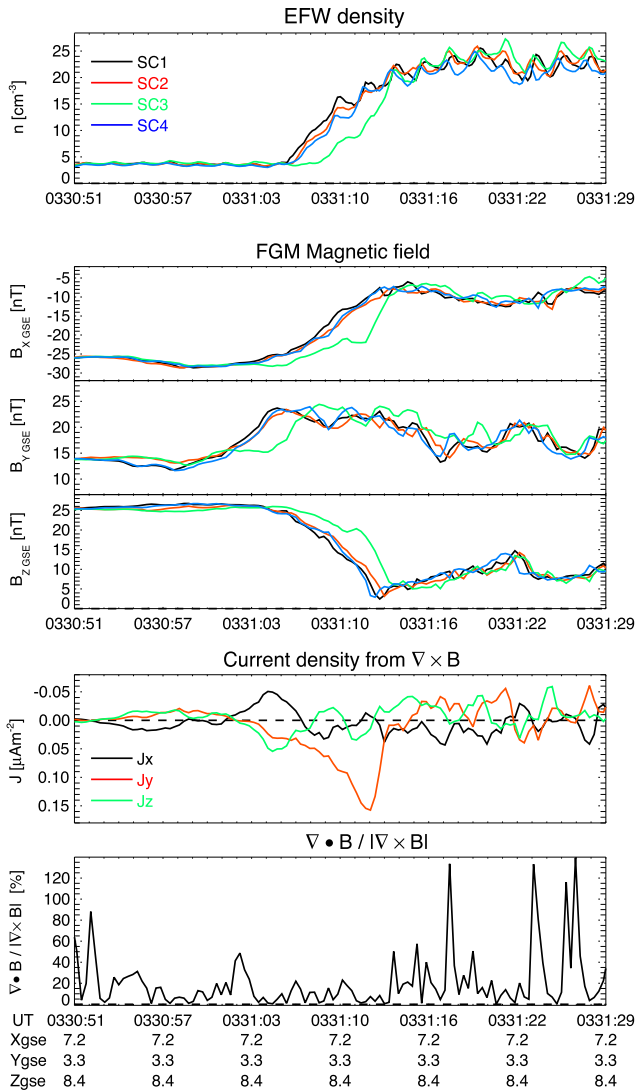


Fig. 14. Overview of magnetopause crossing on 2 March, 2002, around 03:31 UT. Panels show (from top): plasma density from the EFW instrument (the wave-like fluctuations are spin modulations); GSE components of the magnetic field; GSE components of the current density from the curlometer technique; $\nabla \cdot \mathbf{B}/|\nabla \times \mathbf{B}|$, an indicator of the uncertainty in the current estimation (Haaland et al., 2004a). (For interpretation of the references to color in this figure legend, the reader is referred to the web version of this paper.)

exceeded 0.97 in all cases. The results, some of which are shown in Fig. 15, suggest that over a spatial scale of a few 1000 km, the portion of the magnetopause shown in a map was approximately time-stationary. The reconstructed field structures for June 30, 2001 show that on spatial scales of a few 1000 km the magnetopause was bent.

3.7. Surface waves at the magnetopause

Inhomogeneities in the solar wind can locally deform the magnetopause. Even if the wind is steady, magnetic reconnection or excitation of the Kelvin–Helmholtz instability can produce waves along the surface of the magnetopause. An example when the spacecraft were on the

flanks of the magnetosphere at apogee is shown in Fig. 16 from Owen et al. (2004). The magnetopause (defined by the sharp drop of the ≈ 1 keV electrons) is crossed about 20 times in the 1.5 h interval. The spacecraft separation was 2000 km. From timing analysis (Owen et al., 2001) one can determine the direction normal to the surface and its speed. The inbound and outbound magnetopause crossings gave a different normals, suggesting that a wave with wavelength of $\approx 3.4R_E$ passed across the spacecraft at about 65 km/s. The wave was steeper on the leading edge than on the trailing edge, consistent with excitation of the Kelvin–Helmholtz instability.

3.8. Quasi-continuous reconnection at the polar cusp

Magnetic reconnection has been studied by Cluster on both the day and night sides of the magnetosphere. An example observed in the polar cusp is shown in Fig. 17 (Phan et al., 2003). Cluster was crossing the poleward boundary of the cusp and observed first a tailward flow (1), followed by an Earthward flow (2). During this period, B_z was northward. These flows were consistent with reconnection poleward of the cusp under northward interplanetary magnetic field. Simultaneous with these observations, the IMAGE spacecraft observed a bright spot in the auroral zone indicating that accelerated ions were located on the same field lines. This was the first direct evidence that proton aurora are produced by reconnection on the magnetopause at the dayside cusp.

3.9. Reconnection in the magnetotail tail

Cluster has observed several events in the magnetotail that suggest the presence of magnetic reconnection. The right panel of Fig. 18 shows one example from August 17, 2001; a schematic representation of an interpretation of the Cluster measurements is shown in the left panel of the figure. Various regions (I–IV) are noted in both panels. The interpretation of the event is that Cluster detected Hall currents, which indicate that the ions are demagnetized.

On October 1, 2001, Cluster encountered another neutral sheet event that has been studied extensively by Runov et al. (2003). The left top panels of Fig. 19 shows B_y as a function of B_x during two crossings of the neutral sheet. During the first crossing (on the left) B_y changes from being positive at $B_x < 0$ (northern hemisphere) to negative at $B_x > 0$ (southern hemisphere). The other crossing (right panel) is characterized by positive B_y at $B_x > 0$ and negative B_y at $B_x < 0$. This event is also consistent with the presence of a Hall current system that is reversed on the other side of the reconnection point (Sonnerup, 1979). A sketch of the reconnected current sheet structure including the Hall currents (green) near the X-line is shown at the bottom left of Fig. 19. Accelerated plasma is observed on each side of the reconnection point as indicated by the purple arrows.

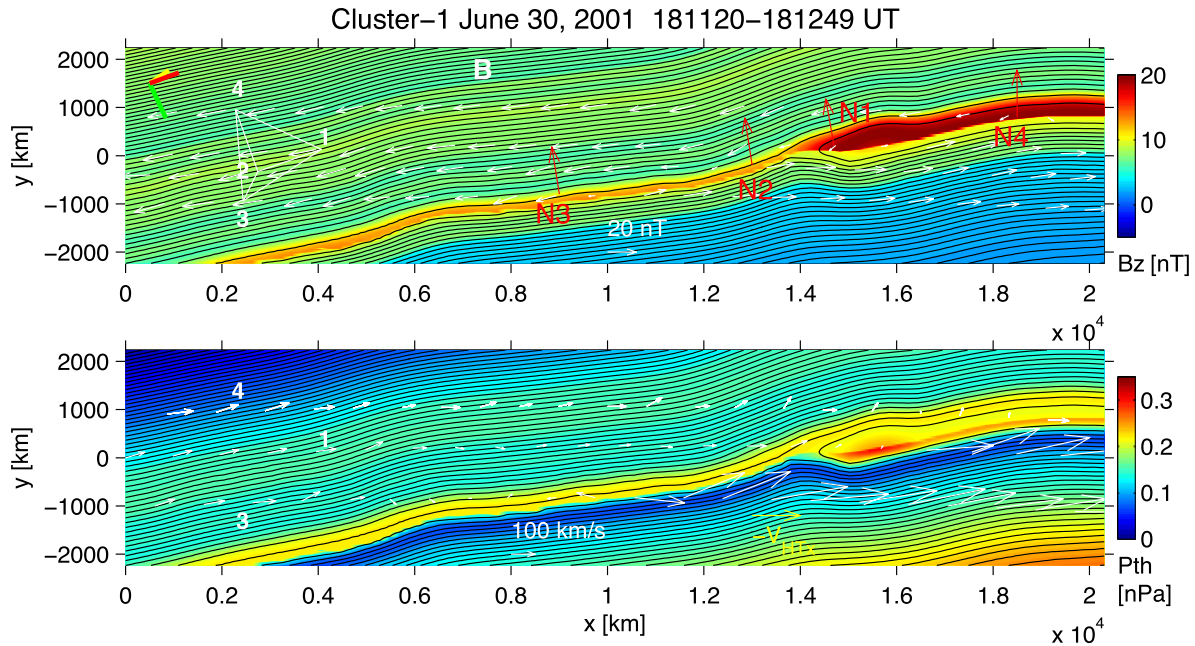


Fig. 15. Magnetic transect (top) and plasma pressure distribution (bottom) obtained by using time-varying deHoffmann-Teller frame velocity for the C1 magnetopause crossing on June 30, 2001. Contours describe the transverse magnetic field lines. In this reconstruction plane, the spacecraft generally moved from left to right. The magnetosheath, ($B_x < 0$; $B_y < 0$) is on the upper left side and the magnetosphere ($B_x > 0$; $B_y > 0$) on the lower right side. In the top panel, B_z is shown in color as indicated by the color bar; the four spacecraft tetrahedron configuration is shown by white lines. The measured magnetic field vectors are projected as white arrows along the spacecraft trajectories. The normal vectors, N1–N4, are projected as red arrows. Line segments in the upper left corner are projections of GSE unit vectors, X (red), Y (green), and Z (yellow), onto the x – y plane. In the bottom panel, the plasma pressure is shown in color. The ion bulk velocity vectors from CIS/HIA (C1 and C3) or CIS/CODIF (C4), transformed into the accelerating deHoffmann-Teller frame, are projected as white arrows (Hasegawa et al., 2004). (For interpretation of the references to color in this figure legend, the reader is referred to the web version of this paper.)

3.10. Traveling compression regions in the tail

Traveling compression regions (TCRs) may be another manifestation of magnetic reconnection and associated flux tubes. On September 19, 2001, Cluster observed small traveling compression regions (Fig. 20). From these data it was possible to determine directly their speed and direction of propagation as well as the amplitude of the underlying bulge in the plasma sheet (Slavin et al., 2003). The time-of-flight speeds derived from the arrival times of the magnetic perturbations at the different Cluster spacecraft yielded a mean speed of 413 km/s. For two of the TCRs, C1, C2 and C4 were located so close to the plasma sheet that they were immersed in the central plasma sheet plasma as the TCR swept over Cluster 3. These observations demonstrate that small TCRs are caused by moving bulges in the plasma sheet–lobe interface.

3.11. Location of the sources of continuum and chorus radio emissions

Cluster offers the first possibility of comparing non-thermal terrestrial continuum radiation from similarly equipped nearby observation points. Analysis using data from the four spacecraft has located the sources of this

radiation (Fig. 21). The spacecraft antenna spin planes provide redundant two-dimensional views of the propagation path of the radiation and source location. The four cases studied (two of them taken near apogee, the other two near perigee) have confirmed general properties derived from previous observations: trapping in the lower frequency range, radiation escaping into the magnetosheath region in the higher frequency range. All propagation directions are compatible with source positions in the plasmopause region, however, at a significant distance from the equator in one case. The observations have also revealed that small-scale density irregularities are important to the local amplification of continuum radiation (Décr  au et al., 2004).

A recent analysis of discrete chorus emissions using WBD from the four Cluster spacecraft by Inan et al. (2004) revealed a rather unexpected frequency difference of around 1 kHz between nearly identical discrete elements observed on different spacecraft. This frequency difference is a consequence of rapid motion ($\approx 20,000$ – $25,000$ km/s) of highly localized source region(s) of chorus of 400–1700 km in extent along the field line (but less than 100 km transverse to the field). The differences in frequency, as well as the different times of arrival of the emissions at different spacecraft, provided an opportunity to estimate the source characteristics using a

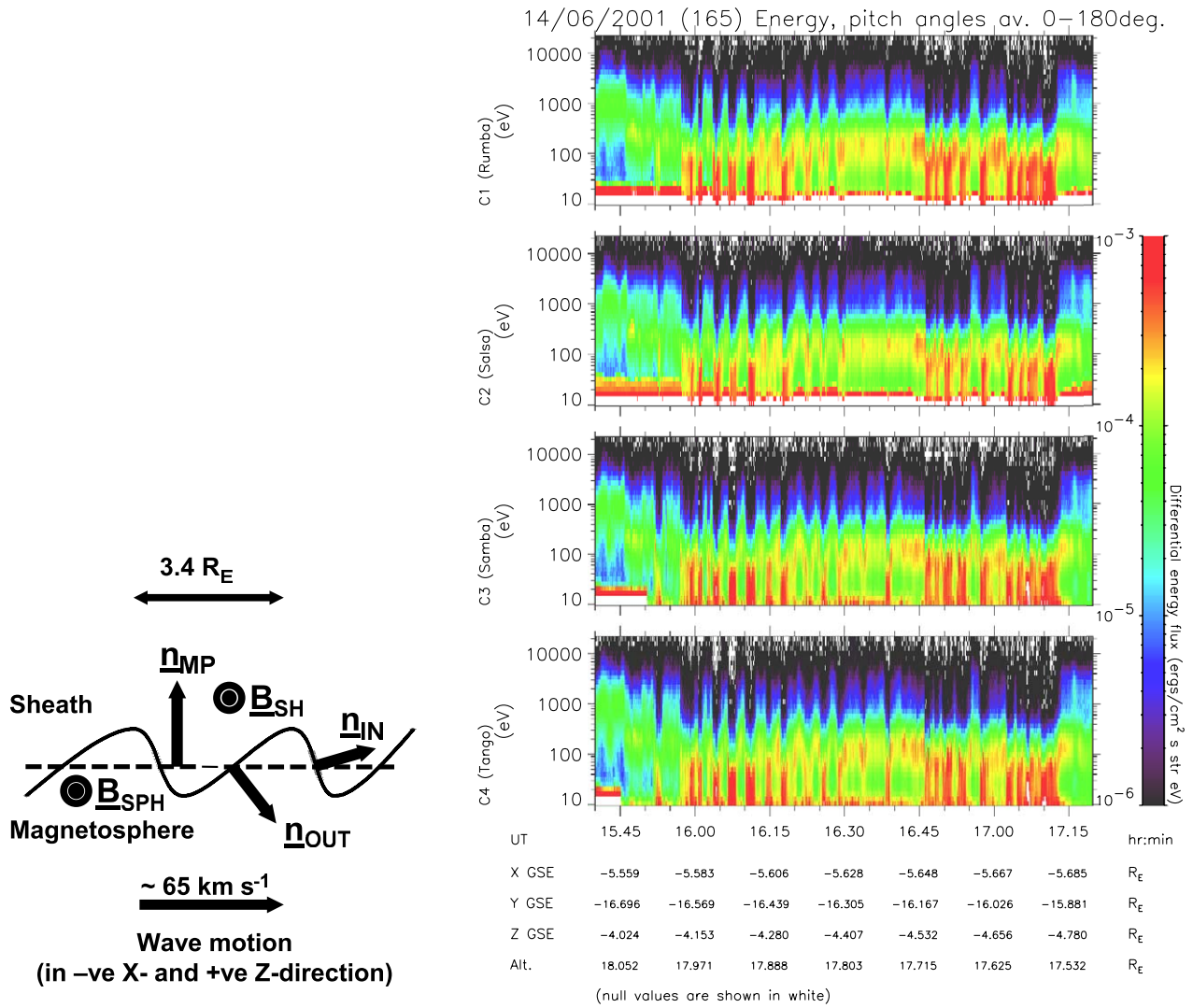


Fig. 16. Left: schematic of a wave propagating along the model magnetopause (dashed line) at about 65 km/s. Right: electron color spectrogram on the four Cluster spacecraft on May 14, 2001 during a magnetopause crossing. High fluxes below 100 eV in red indicate the magnetosheath and low fluxes above 100 eV indicate the magnetosphere (Owen et al., 2004). (For interpretation of the references to color in this figure legend, the reader is referred to the web version of this paper.)

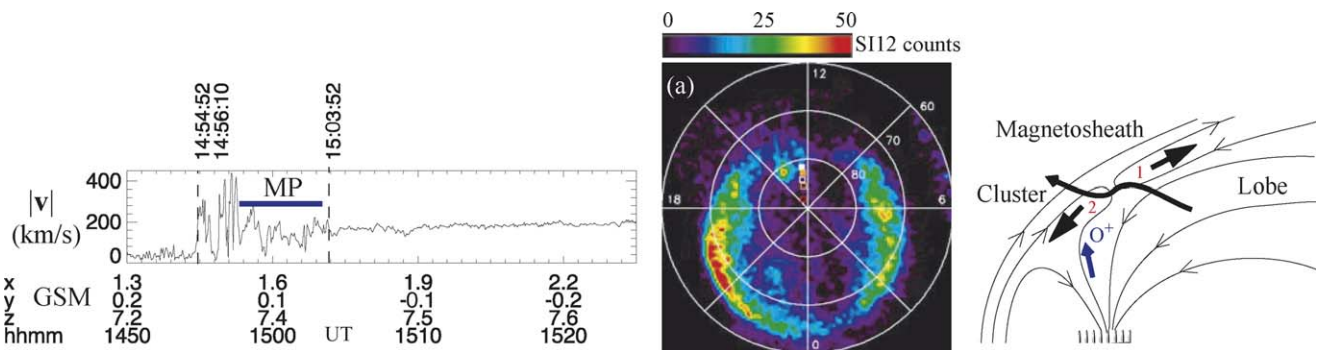


Fig. 17. Left: Cluster observations of ion jetting. Center: image observations. Right: schematic of the location of the cusp and auroral activity (Phan et al., 2003).

model involving rapidly moving sources traveling at speeds comparable to the parallel resonant velocity of counterstreaming electrons moving along the local mag-

netic field. The analyses provide the first experimental evidence that the sources that generate the discrete chorus emissions are in rapid motion.

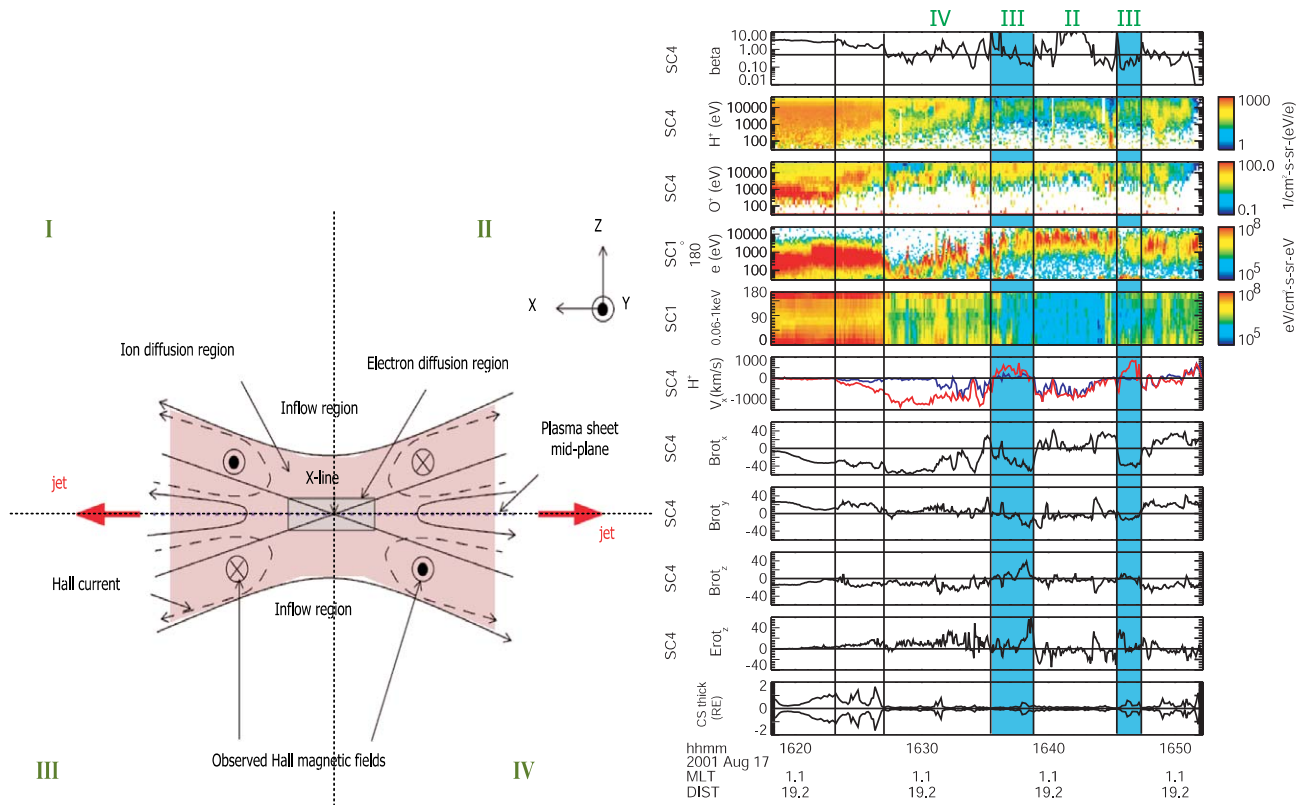


Fig. 18. Left: a schematic of reconnection. The ion diffusion region is marked by the shaded red area and the smaller electron diffusion region is a grey box. The system of Hall currents induce a quadrupolar out-of-plane magnetic field pattern. Each of the four quadrants, designated I, II, III and IV, satisfies a unique combination in the sign of the B_x , B_y , B_z , V_x components. Right: Cluster data for the period 16:15–16:55 UT, August 17, 2001; (1) C4 plasma beta; (2) C4 CODIF H⁺ energy spectra; (3) C4 CODIF O⁺ energy spectra; (4) C1 180° pitch angle PEACE energy spectra; (5) C1 PEACE pitch angle spectra for the 60 eV–1 keV energy range; (6) C4 CODIF H⁺ V_x velocity component in GSE (red is total V_x ; black is $V_x \parallel B$). Panels 7–9: C4 FGM magnetic field in the minimum variance coordinates; (10) C4 EFW electric field E_z in minimum variance coordinates; (11) current sheet thickness. The first vertical line is the onset of tailward flows. Shaded areas indicate periods during which earthward flows were observed. The roman numbers indicate the quadrant in which the spacecraft was located. (Figure courtesy of C. Mouikis.) (For interpretation of the references to color in this figure legend, the reader is referred to the web version of this paper.)

3.12. Studies of auroral kilometric radiation

The Cluster Wideband Data instrument has been used to determine the locations of auroral kilometric radiation (AKR) (Mutel et al., 2003) using very long baseline interferometry, which involves cross-correlating individual AKR bursts from all six Cluster baselines using time and frequency filtered waveforms. The resulting differential delay peaks are used to determine source locations with an uncertainty as small as 500 km in a plane perpendicular to the source-spacecraft line of sight, or about 200 km when the burst position is projected onto the auroral zone along the magnetic field lines passing through the source. The uncertainty along the line of sight is much larger, but is mitigated by assuming that the emission arises from a height corresponding to the local electron gyrofrequency.

Between July 10, 2002 and January 22, 2003, over 1700 locations of individual AKR bursts were determined. In general, the AKR burst locations lie along magnetic field lines that map onto the nighttime auroral zone, consistent with previous studies. In the northern hemisphere there is a

strong tendency for AKR burst locations to be centered within the auroral oval and in the evening sector (Fig. 22).

The distribution of AKR auroral footprint locations at each epoch had an overall spatial scale between 1000 and 2000 km, much larger than the positional uncertainty of an individual AKR burst location magnetic footprint, but a small fraction of the auroral oval. This indicates that on a timescale of 1–3 h conditions for suitable generation of AKR emission are found on only a fraction of all magnetic field lines crossing through the auroral oval. For two of the six epochs, there was a significant drift in the mean location of AKR activity over a period of 1–2 h. The drift was predominantly in latitude at one epoch and in longitude at the other, with average drift speed $V \approx 80$ – 90 m s^{-1} at the AKR emission location (Mutel et al., 2003).

4. Cluster science data system

The Cluster science data system has been set-up to distribute quicklook and processed data to all Cluster Principal and Co-Investigators, as well as to the scientific community. The Cluster data system is distributed

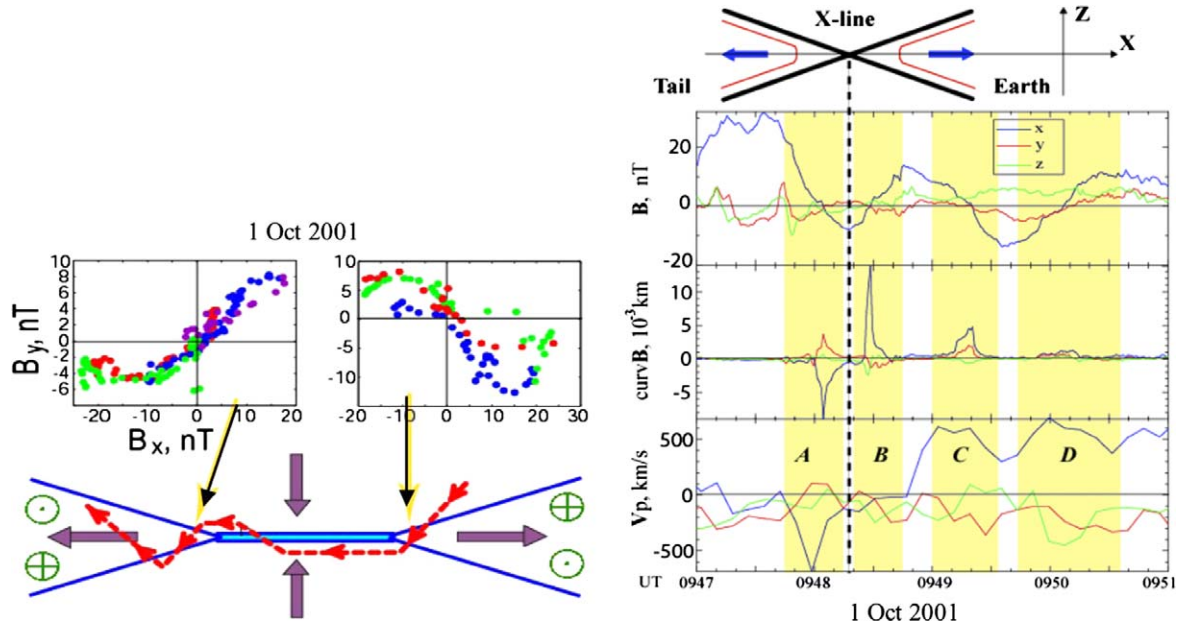


Fig. 19. Left: two crossings of a thin (≈ 500 km wide) neutral sheet on October 1, 2001. At the top are the magnetic field data as measured and below is a sketch showing the inferred reconnection bifurcated geometry and the respective trajectory of Cluster (dashed red line) (Runov et al., 2003). The out-of-plane magnetic field, ΔB_y , indicates that ions are demagnetized. Right: the top panel shows the vector components of the magnetic field at the Cluster barycenter. There are four current sheet traversals during this time period. Also shown are the magnetic field line curvature, $(\mathbf{b} \cdot \nabla)\mathbf{b}$. The field line curvature and the bottom panel showing the plasma flow behavior as expected if an X-line were moving tailward over the spacecraft. (For interpretation of the references to color in this figure legend, the reader is referred to the web version of this paper.)

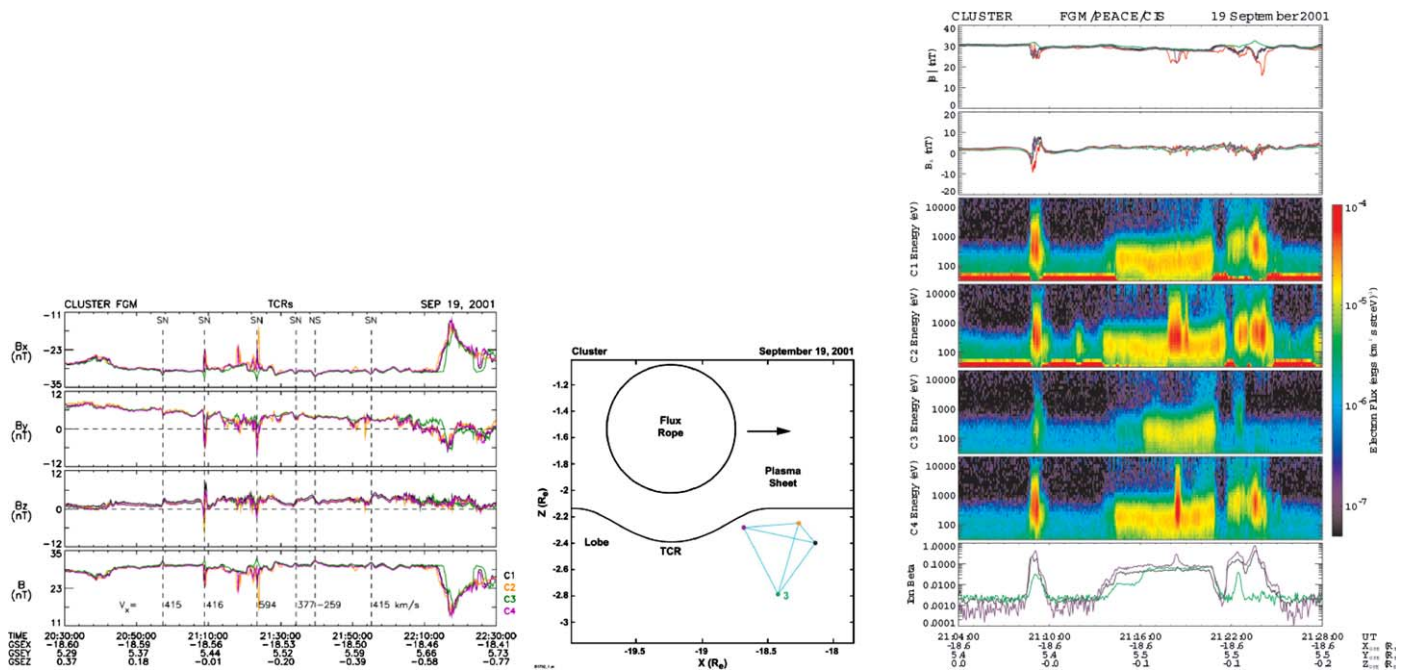


Fig. 20. Left: Cluster FGM observations of a series of traveling compression regions observed in the tail on September 19, 2001. Center: schematic view of a bulge in the plasma sheet (TCR) produced by an earthward moving flux tube. Right: CIS, FGM, and PEACE observations of two TCRs (Slavin et al., 2003).

among nine data centers located in Austria, China, France, Germany, Hungary, Netherlands, Sweden, United-Kingdom and United-States. Each data center stores the full database of processed and validated data from all instruments. Data from February 2001 are available

through the web at <http://sci2.estec.esa.nl/cluster/csds/csds.html>. Quicklook plots are available a few hours to a few days after data acquisition. These quicklook data include time series plots and spectrograms from most of the instruments.

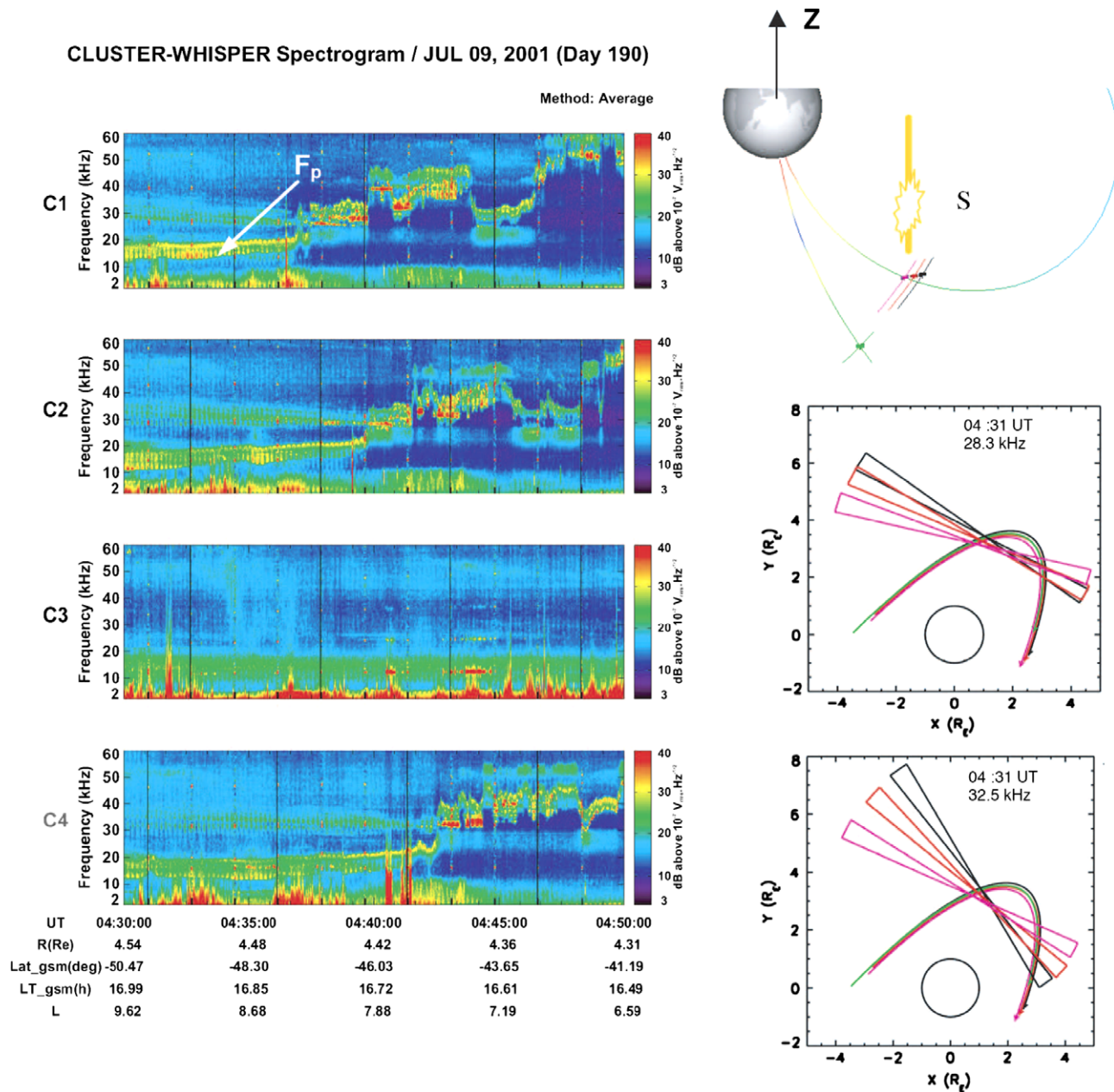


Fig. 21. Direction analysis for the July 9, 2001 event. Left: frequency/time spectrograms measured by the four Cluster spacecraft at the approach of the plasmasphere. Orbital parameters are indicated for C4. Right, top: orbit elements in a meridian plane from 04:25 to 04:55 UT. Spacecraft are moving from the southern to northern hemisphere. Field lines crossed by C4 (purple) and C3 (green) are drawn at 04:45 UT. The orange segment and patch indicate source positions as discussed in Décréau et al. (2004). Right, bottom: triangulation at two frequencies from C1, C2, and C4. Each direction is indicated as the angle spanned over 5° about the central direction. All point to a source region located earthward from the orbit in the x - y GSE-plane shown (orbits and direction angles are projected onto the plane) (Décréau et al., 2004). (For interpretation of the references to color in this figure legend, the reader is referred to the web version of this paper.)

4.1. Public access to other data sets

The PI teams are also distributing other Cluster data sets, including particle spectrograms, high resolution data, enhanced prime parameters data, and summary plots. The web links are:

ASPOC: <http://saturn.iwf.oeaw.ac.at/acdc/acdc.html>
(raw data)

CIS: http://cis.cesr.fr:8000/CIS_sw_home-en.htm (6-h spectrograms)

EDI: http://ediweb.sr.unh.edu/edi_pp_data.html (prime parameters)

EFW: <http://www.cluster.irfu.se/efw/data/spinfit/index.html> (E_x , E_y at 4 s resolution)

FGM: http://jakal.sp.ph.ic.ac.uk/fgm/fgm_pp_data.php
(prime parameters)

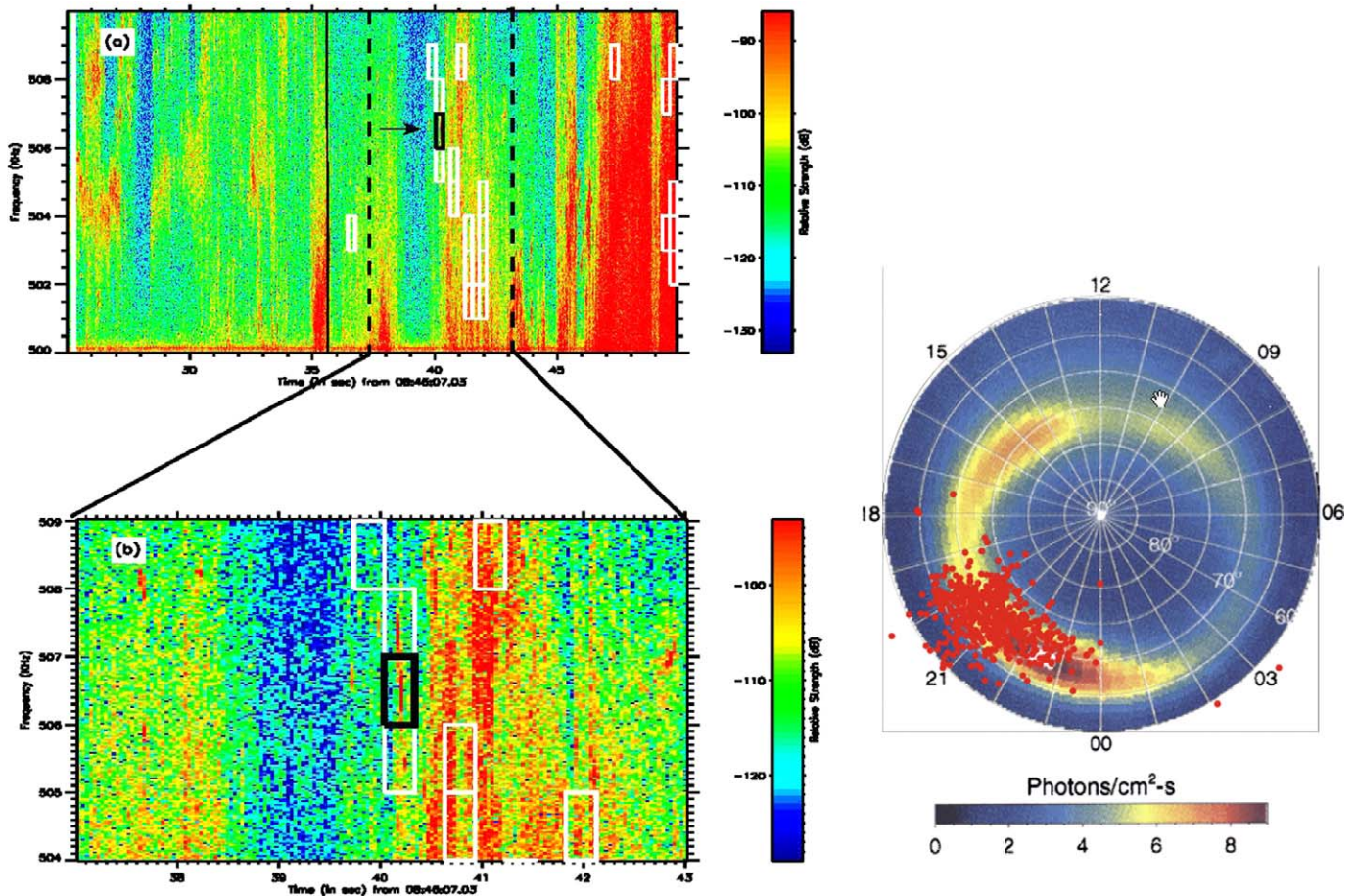


Fig. 22. Left panels: dynamic spectrum of AKR bursts, 500–510 kHz over 25 s on July 10, 2002 starting at 08:47:03 UT. Top: the 25 sec spectrum. Bottom: 6 s in more detail. The black boxed area is an AKR burst whose crosscorrelation function on all six baselines and derived location loci were determined. The white boxes are other regions for which burst locations were determined. The logarithmic scale shows the relative burst flux density. Right: location of isolated AKR bursts (Mutel et al., 2003).

PEACE: <http://cluster2.space.swri.edu/> (high resolution spectrograms from PEACE and other instruments)

RAPID: <http://www.linmpi.mpg.de/english/projekte/cluster/download/DownLd.cgi?cmd=Form> (high resolution data)

STAFF: <http://www.cetp.ipsl.fr/CLUSTER/accueil/framepa.html> (spectrograms)

WBD: <http://www-pw.physics.uiowa.edu/plasma-wave/istp/cluster/> (spectrograms)

WHISPER: <http://www.whisper.cnrs-orleans.fr/> (spectrograms)

4.2. Cluster active archive

In February 2003, the Cluster Project received approval from the ESA Science Program Committee to create a public Cluster Active Archive (CAA) to contain processed and validated high-resolution scientific data, as well as raw data, processing software, calibration data and documentation from all the Cluster instruments.

The CAA is being established and maintained under the overall control of ESA. The design phase for the

archive started in February 2003 and is being followed by a development and implementation phase during 2004.

Data from all instruments should be incorporated into the database at an average rate of two years of data per calendar year. It is anticipated that all the data through the end of 2005 will be in the archive by the end of 2006. Reprocessing and finalization of the archive will occur in 2007. The archive is publically accessible at <http://caa.estec.esa.int/caa/>.

5. Conclusions

After more than five years of operations, the Cluster spacecraft have made substantial advances in magnetospheric physics. For the first time plasma structures in the magnetosphere and solar wind have been studied in three dimensions. During 2005 the separation of the spacecraft were increased to 10,000 km. Configurations other than regular tetrahedra are being used to maximize the science in both the solar wind and plasma sheet. Cluster operations are funded to the end of 2007 and a further extension through 2009 is likely.

Cluster is now complemented by the Chinese Double Star mission which consists of an equatorial spacecraft TC-1 ($550 \times 66,970$ km, 28.5° inclination) and a polar spacecraft TC-2 ($700 \times 39,000$ km, 90° inclination). The Double Star orbits have been designed to maximize conjunctions with Cluster in the plasma sheet and in the polar cusp. Half of the Double Star payload consists of spare or duplicate Cluster instruments.

Acknowledgment

This work was supported, in part, by NASA.

References

- Bale, S.D., Mozer, F.S., Horbury, T.S. Density-transition scale at quasiperpendicular collisionless shocks. *Phys. Rev. Lett.* 91, doi:10.1103/PhysRevLett.1191.265004, 2003.
- Décéau, P., Ducoin, C., Le Rouzic, G., et al. Observation of continuum radiations from the Cluster fleet: first results from direction finding. *Ann. Geophys.* 22, 2607–2624, 2004.
- Dunlop, M.W., Balogh, A., Glassmeier, K.H. Four-point Cluster application of magnetic field analysis tools: the discontinuity analyzer. 10.1029/2001JA005089, 2002.
- Escoubet, C.P., Fehringer, M., Goldstein, M. The Cluster mission. *Ann. Geophys.* 19, 1197–1200, 2001.
- Giacalone, J., Schwartz, S.J., Burgess, D. Observations of suprathermal ions in association with SLAMs. *Geophys. Res. Lett.* 20 (2), 149–152, 1993.
- Glassmeier, K.H., Motschmann, U., vom Stein, R. Mode recognition of mhd wave fields at incomplete dispersion measurements. *Ann. Geophys.* 13, 76–83, 1995.
- Haaland, S., Sonnerup, B.U.Ö., Dunlop, M.W., Georgescu, E., Paschmann, G., Klecker, B., Vaivads, A. Orientation and motion of a discontinuity from cluster curlometer capability: minimum variance of current density. *Geophys. Res. Lett.* 31 (10), 10804, doi:10.1029/2004GL020001, 2004a.
- Haaland, S.E., Sonnerup, B.U. Ö., Dunlop, M.W., et al. Four-spacecraft determination of magnetopause orientation, motion and thickness: comparison with results from single-spacecraft methods. *Ann. Geophys.* 22, 1347–1365, 2004b.
- Hasegawa, H., Sonnerup, B.U.Ö., Dunlop, M.W., et al. Reconstruction of two-dimensional magnetopause structures from Cluster observations: verification of method. *Ann. Geophys.* 22, 1251–1266, 2004.
- Inan, U.S., Platino, M., Bell, T.F., Gurnett, D.A., Pickett, J.S. Cluster measurements of rapidly moving sources of ELF/VLF Chorus. *J. Geophys. Res.* 109 (A5), A05214, doi:10.1029/2003JA010289, 2004.
- Kucharek, H., Möbius, E., Scholer, M., et al. On the origin of field-aligned beams at the quasi-perpendicular bow shock: multi-spacecraft observations by Cluster. *Ann. Geophys.* 22, 2301–2308, 2004.
- Lucek, E.A., Horbury, T.S., Balogh, A., Dandouras, I., Reme, H. Cluster observations of structures at quasi-parallel bow shocks. *Ann. Geophys.* 22 (7), 2309–2313, 2004.
- Motschmann, U., Glassmeier, K.-H., Pinçon, J.-L., Multi-spacecraft filtering: Plasma mode recognition, in: Paschmann, G. Daly, P. (Eds.), *Analysis Methods for Multispacecraft Data*, vol. SR-001, pp. 71–89. ESA, 1998.
- Motschmann, U., Woodward, T.I., Glassmeier, K.-H., Southwood, D.J., Pinçon, J.-L. Wavelength and direction filtering by magnetic measurements at satellite arrays: generalized minimum variance analysis. *J. Geophys. Res.* 101, 4961–4965, 1996.
- Mutel, R.L., Gurnett, D.A., Christopher, I.W., Pickett, J.S., Schlax, M. Locations of auroral kilometric radiation bursts inferred from multi-spacecraft wideband cluster VLBI observations 1. description of technique and initial results. *J. Geophys. Res.* 108 (11), 1398, doi:10.1029/2003JA010011, 2003.
- Owen, C.J., Fazakerley, A.N., Carter, P.J., et al. Cluster peace observations of electrons during magnetospheric flux, transfer events. *Ann. Geophys.* 19, 1509–1522, 2001.
- Owen, C.J., Taylor, M.G.G.T., Krauklis, I.C., et al. Cluster observations of surface waves on the dawn flank magnetopause. *Ann. Geophys.* 22, 971–983, 2004.
- Phan, T., Frey, H.U., Frey, S., Peticolas, L., Fuselier, S., Carlson, C., Rème, H., Bosqued, J.-M., Balogh, A., Dunlop, M., Kistler, L., Mouikis, C., Dandouras, I., Sauvaud, J.-A., Mende, S., McFadden, J., Parks, G., Moebius, E., Klecker, B., Paschmann, G., Fujimoto, M., Petrinc, S., Marcucci, M.F., Korth, A., Lundin, R. Simultaneous Cluster and IMAGE observations of cusp reconnection and auroral proton spot for northward IMF. *Geophys. Res. Lett.* 30 (10), doi:10.1029/2003GL016885, 2003.
- Pinçon, J.-L., Lefeuvre, F. Local characterization of homogeneous turbulence in a space plasma from simultaneous measurement of field components at several points in space. *J. Geophys. Res.* 96, 1789–1802, 1991.
- Robert, P., Dunlop, M.W., Roux, A., Chanteur, G. Accuracy of current density determination, in: Paschmann, G., Daly, P.W. (Eds.), *Analysis Methods for Multi-Spacecraft Data*. ESA Publ, SR-001, Noordwijk, Netherlands, pp. 395–418, 1998.
- Runov, A., Nakamura, R., Baumjohann, W., Treumann, R.A., Zhang, T.L., Volwerk, M., Vörös, Z., Balogh, A., Glaßmeier, K.-H., Klecker, B., Rème, H., Kistler, L. Current sheet structure near magnetic x-line observed by Cluster. *Geophys. Res. Lett.* 30 (11), 1579, doi:10.1029/2002GL016730, 2003.
- Sahraoui, F., Pinçon, J.L., Belmont, G., Rezeau, L., Cornilleau-Wehrin, N., Robert, P., Mellul, L., Bosqued, J.M., Balogh, A., Canu, P., Chanteur, G. Ulf wave identification in the magnetosheath: The k-filtering technique applied to Cluster II data. *J. Geophys. Res.* 108 (A9), 1335, doi:10.1029/2002JA009587, 2003.
- Scholer, M., Burgess, D. The role of upstream waves in supercritical quasi-parallel shock re-formation. *J. Geophys. Res.* 97 (A6), 8319–8326, 1992.
- Schwartz, S.J. Magnetic field structures and related phenomena at quasi-parallel shocks. *Adv. Space Res.* 11 (9), 231–240, 1991.
- Schwartz, S.J., Burgess, D. Quasi-parallel shocks – a patchwork of 3-dimensional structures. *Geophys. Res. Lett.* 18 (3), 373–376, 1991.
- Slavin, J.A., Lepping, R.P., Gjerloev, J., Goldstein, M.L., Fairfield, D.H., Acuna, M.H., Balogh, A., Dunlop, M., Kivelson, M.G., Khurana, K., Fazakerley, A., Owen, C.J., Reme, H., Bosqued, J.M. Cluster electric current density measurements within a magnetic flux rope in the plasma sheet. *Geophys. Res. Lett.* 30 (7), doi:10.1029/2002GL016411, 2003.
- Sonnerup, B.U.Ö. Magnetic field reconnection, in: Kennel, C.F. et al. (Eds.), *Solar System Plasma Physics*. North-Holland Publishing Company, Amsterdam, pp. 45–108, 1979.